IEEE Access
Multidisciplinary | Rapid Review | Open Access Journal

IEEE ENGINEERING IN MEDICINE AND BIOLOGY SOCIETY SECTION

Received March 11, 2020, accepted April 5, 2020, date of publication April 21, 2020, date of current version May 5, 2020.

Digital Object Identifier 10.1109/ACCESS.2020.2989175

Prediction-Based Reversible Watermarking of CT Scan Images for Content Authentication and Copyright Protection

NISAR AHMED MEMON AND ALI ALZAHRANI, (Member, IEEE)

Department of Computer Engineering, College of Computer Sciences and Information Technology (CCSIT), King Faisal University, Al-Ahsa 31982, Saudi Arabia

Corresponding authors: Nisar Ahmed Memon (nmemon@kfu.edu.sa) and Ali Alzahrani (aalzahrani@kfu.edu.sa)

This work was supported by the Deanship of Scientific Research, King Faisal University, through the Nasher Track under Grant 186145.

ABSTRACT In the application of teleradiology, radiologists located at different geographical locations around the globe, exchange Computed Tomography (CT) scan images along with relevant patient information for diagnosis as well as therapeutic measures. However, when these images are exchanged over public networks like the Internet, two important issues are created: content authentication and copyright protection. In this paper, a novel high capacity reversible watermarking scheme for CT Scan images is presented which is based on the region of interest (ROI) and region of non-interest (RONI) watermarking. The scheme embeds and extracts the secret data into the input CT scan image as well as restores the image to its pristine state at the receiving end. After segmenting the host image into the ROI and RONI regions, the scheme implants a fragile watermark (FW) into the ROI to check the integrity of the ROI and a robust watermark (RW) into the RONI for copyright protection. The novelty of the proposed system is in two fold. First, it takes advantage of the segmentation algorithm to avoid the additional overhead of information about the vertices usually required at the receiving end in order to select the ROI. Secondly, it takes advantage of the prediction-based reversible watermarking to avoid additional overhead of location map, which is usually required for reversibility in most of the reversible medical image watermarking techniques. Experimental results show that the proposed system outperforms medical image watermarking techniques recently reported in the literature in terms of embedding capacity and imperceptibility of watermarked image.

INDEX TERMS Prediction-based reversible watermarking, authenticity, confidentiality, CT scan medical images, ROI and RONI.

I. INTRODUCTION

In teleradiology, CT Scan images of patients along with the patient-related data are shared by radiologists over public networks like the Internet for clinical interpretation with other radiologists and physicians. However, this transmission of images and patient data is not safe until any strong layer of protection is used. Tampering these images could result in misdiagnosis [1]. Also, tampering of the images can create different legal and ethical issues such as image retention and fraud, privacy and illegal handling, etc. This is because security measures related to teleradiology are still the same and have not changed according to modern requirements of security and privacy of medical records [2]. Thus, in teleradiology, which is a successful eHealth service presently, security and privacy of radiological images such as CT Scan images has become a very important issue [3], [4].

Besides images, patient information is also another important entity in teleradiology. In teleradiology, this information is generally stored electronically and is referred as Electronic Patient Record (EPR). The EPR usually contains details of the patient, like name, age, sex, diagnosis report and hospital information where the image was produced [5].

Digital image watermarking techniques [6]–[10] have attractive properties to resolve such issues. Digital image watermarking can be carried out in two domains: spatial domain and frequency domain. In spatial domain watermarking techniques [11]–[13] secret data is directly implanted into the cover image by changing the pixel values. In frequency domain watermarking techniques [14]–[16], the cover image

The associate editor coordinating the review of this manuscript and approving it for publication was Kin Fong Lei.

is first transformed into some frequency domain and then secret data is implanted by changing the values of frequency coefficients.

Some other class of watermarking techniques are irreversible and reversible watermarking techniques. In irreversible watermarking techniques [14] lossless recovery of host image is not possible while in reversible watermarking techniques [15]–[17] lossless recovery of host image is possible and it can be recovered to its pristine state. Reversible watermarking techniques are more suitable for medical images [18].

Based on application, watermarking techniques can be divided into two categories: (i) Robust watermarking and (ii) Fragile watermarking. In robust watermarking [14]–[16] the main focus is on the robustness of hidden data, i.e how much implanted data can sustain any legitimate and illegitimate attacks during transmission, thus these techniques are used for copyright protection. In fragile watermarking techniques [11]–[13] focus is on the detection of tampering areas in the image, if the image is tampered with during transmission by the invader. Thus these techniques are particularly used for checking the integrity of the content of the medical image.

Generally, medical image consists of ROI and RONI. ROI is a vital part of diagnosis. Thus, during watermarking, hidden information is implanted in the ROI in such a way that visual quality of ROI should not be too much degraded. The recovery information of the ROI is implanted into the RONI [19]–[21]. While transmitting the medical image from one place to another place, if the ROI has been tampered, the tampered area is replaced with recovery information previously implanted in the RONI.

In this paper, a novel watermarking system for medical images based on prediction-based reversible watermarking is proposed for obtaining the following objectives:

(1) Recovering the ROI at the receiving end with zero loss if it is tampered during transmission.
(2) Recovering the RONI by employing the prediction based reversible watermarking.
(3) Diagnosis value of the ROI will not be compromised.
(4) Having the good visual quality of medical images after watermarking.
(5) Providing secrecy and privacy of patient data.
(6) Providing a mechanism for assuring the integrity of medical images.

This paper is further organized as follows: Section 2 covers the state-of-art medical image watermarking techniques currently reported in the literature. Section 3 explains the tools and techniques used in the proposed research work. In section 4, the proposed system has been explained. Section 5 illustrates the experimental results. Finally conclusions are made in Section 6.

II. RELATED WORK

A large number of blind, fragile and reversible watermarking techniques were recently presented for content authentication and copyright protection of medical images. Few related techniques are described as under.

Thabit and Khoo [22] presented a reversible medical image authentication technique which addresses the issue of illegitimate attacks on watermarked images and the robustness of authentication technique to withstand against these illegitimate attacks. The proposed technique utilizes Slantlet Transform (SLT) to embed watermark information in the ROI and RONI regions. The ROI is divided into non-overlapping blocks of size 16×16 and the average intensity of each block is calculated. After that, Integer Wavelet Transform (IWT) coefficients were exploited to get recovery information for ROI. The extracted information from ROI is implanted in RONI. The main limitations of the technique are: (1) tampered regions cannot be detected without average intensities of blocks and (2) there is a need of additional information at the decoder side along with the watermarked image which increases the unnecessary overhead for the technique.

Eswaraiah and Reddy [23] reported a reversible medical image watermarking scheme which is only reversible for ROI. The scheme will not be able to restore RONI. In this scheme, first, the host image is divided into ROI and RONI. Later by exploiting IWT coefficients recovery information of ROI, hash value and EPR are implanted in RONI. The limitations of this scheme are: (1) more additional overhead information is required at the decoder side for recovering ROI (2) it cannot be applied to the images where ROI size is greater than 20% of the whole image.

Selvam *et al*. [24] reported another reversible medical image watermarking technique based on IWT and Discrete Gould Transform (DGT). The technique provides more embedding capacity and does not require a cover image by the decoder for extracting watermark information. The image can be restored to its pristine state without having any side information. Thus, the technique does not require any additional overhead for reversibility. The limitation of this technique is that even with having low payload embedded in the host image it produces high distortion in the watermarked image.

Parah *et al*. [25] presented a reversible medical image watermarking system for content authentication. The watermarked information is embedded into Intermediate Significant Bit (ISB) instead of LSB to provide safeguards to the watermarked image from LSB removal attacks. The watermarked information is composed of EPR, block checksum, and hospital logo. A pixel-to-Block (PTB) conversion method has been adopted to achieve more embedding capacity. The limitation of this system is that, though the system provides high embedding capacity, but the imperceptibility of the watermarked image is not so high.

Gao *et al*. [26] proposed a reversible medical image watermarking scheme for medical images that uses contrast enhancement and feature-bit matrix features for reversibility. Initially, host image is divided into ROI and RONI regions. Later the hidden information is implanted which is the distortion-less contrast enhancement information of ROI. A feature-bit matrix was produced from ROI and is implanted

in LSBs of RONI to get the reversibility of ROI. The main limitations of this scheme are: (1) Feature-matrix is required for implanting watermarked information in the host image and (2) only ROI can be restored at the receiving end. Thus the scheme is semi-reversible.

Balasamy and Ramakrishnan [27] reported another reversible medical image watermarking approach based on Discrete Wavelet Transform (DWT) and Particle Swarm Optimization (PSO). The PSO has been employed for selecting optimal wavelet coefficients for embedding the hidden information. The decoder does not require external additional information for extracting the watermarked information. The limitation of this approach is that it introduces high distortion in the watermarked image despite the low payloads.

Yang *et al*. [28] presented a reversible medical image watermarking technique which first divides the host image into ROI and RONI. After then the contrast of the ROI region was enhanced by extending the gray values and the data were embedded into the peaks bins of the extended histogram without stretching the histogram bins. The technique reports high values of Peak Signal to Noise Ratio (PSNR) due to the contrast enhancement applied. The limitation of the technique is that the huge amount of data was implanted into RONI without considering the visual quality of the watermarked image.

Atta-ur-Rehman *et al*. [6] proposed a reversible medical image watermarking scheme for the confidentiality of patient data and content authentication of medical images. In this scheme, watermark is first generated chaotically and then it is implanted in the host image by employing a chaotic key. The remaining pixels are then transformed into residues by utilizing the Residue Number System (RNS). A primitive polynomial of degree four is selected for message polynomial to get the remainder. This remainder is XORed with a watermark and is appended with the message. At the decoder side, the validity of the watermark is ensured based on the calculated remainder. The scheme reports a high value of PSNR. The main limitation of this scheme is that it does not support the ROI-based watermarking strategy which makes this scheme incapable of selecting the hiding regions.

Another novel robust medical image watermarking technique was reported by Liu *et al*. [29]. The technique addressed the issue of loss of information during the segmentation process when the input image is segmented in the ROI and RONI regions for embedding the watermark information. The technique is based on recursive dither modulation (RDM). The SLT and SVD are later combined with RDM to achieve image authenticity. The watermark is implanted in the whole image instead of regions to avoid the risk of loss of information due to the segmentation process at the receiving end.

Recently Swaraja *et al.* [30] presented a reversible medical image watermarking scheme based on DWT, Schur Transform and Particle Swarm Bacterial Foraging Optimization Algorithm (PSBFO). The less compression technique Lempel-Ziv-Welch (LZW) was used for reducing the size of watermark and achieving the high embedding capacity which in turn gets high imperceptibility of an output image.

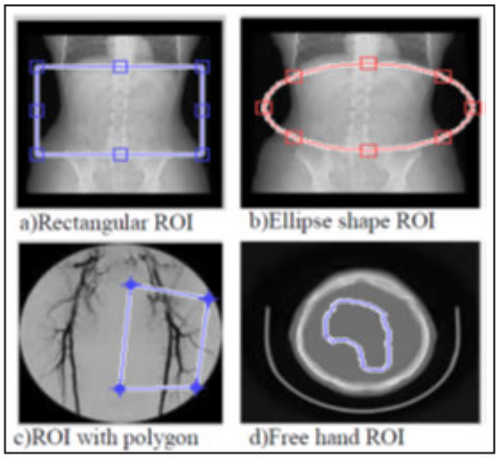

FIGURE 1. Different options used for selecting ROI [31].

After reviewing these techniques, it can be observed that there are some limitations to every technique. In the proposed system, measures have been taken to overcome these limitations.

III. TOOLS AND TECHNIQUES

The following tools and techniques were used in the proposed reversible watermarking system for CT scan medical images.

A. SEGMENTATION OF INPUT CT SCAN IMAGE

In the proposed system, input CT Scan medical image is first segmented into ROI and RONI regions. Generally, in the applications of medical image diagnosis, medical practitioner examines the ROI. Based on his/her choice, the medical practitioner segments the host image into ROI and RONI. In this regard, a number of techniques are used. Some medical practitioners use geometrical shapes, like, square, ellipse or free polygon for selecting ROI, while others use a freehand tool [31] for selecting ROI. Fig. 1 depicts the number of methods used for selecting ROI. In lung CT Scan medical images, the lung parenchyma of the human body generally, is the choice of a medical practitioner for a diagnosis. Keeping in view this point, we have used Algorithm 1 for segmentation as reported in [32] for dividing the input CT Scan image into ROI and RONI regions.

B. LSB SUBSTITUTION METHOD

For reducing the computational cost, the LSB substitution method was used for embedding the watermarked information, which is very simple and can easily be implemented as described in [33]. In the LSB substitution method, the data is implanted in different bit planes of the input image by replacing the LSBs with a payload.

Experiments show that implanting the watermarked information in the lower bit planes yield higher values of PSNR, while higher bit planes report lower values of PSNR [34], as obtained from the results of the experiment shown in Fig.

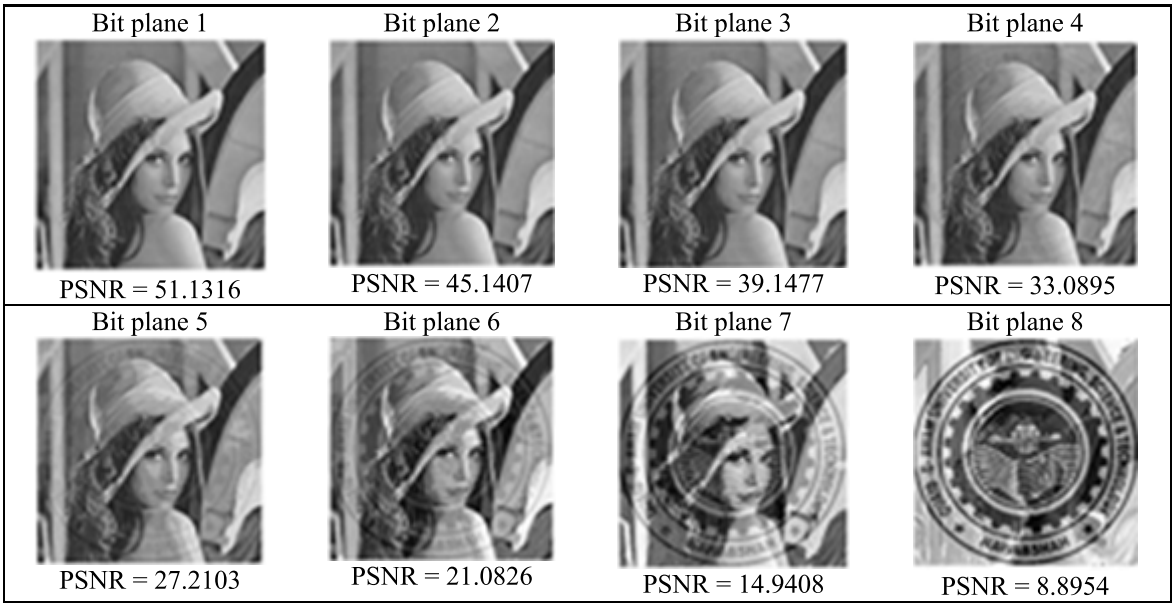

FIGURE 2. Different PSNR values of watermarked images after embedding the payload in 8 different bit planes.

2. For this, a logo of some university, which is the binary image of size 256 × 256 pixels was embedded in standard Lena image of the same size. The noise produced in the input image after implanting the payload in each bit plane was measured and the results are shown in Fig. 2. Fig. 2 portrays that the lowest bit planes show the higher values of PSNR i.e greater than benchmark value of 38.00 (decibels) dB and the logo is completely hidden in the image. Whereas, higher bit planes show the lower values of PSNR and the logo is more visible in these bit planes. As Eswaraiah and Reddy [23] explained that a medical image watermarking technique is more effective if the value of PSNR of watermarking image is greater than 40 dB. Keeping in view the results shown in Fig. 2, we selected the bit plane 1 for embedding the watermark information in ROI and both bit planes 1 and 2 for embedding watermarked information in the RONI. Both bit planes report PSNR values of more than 40 dB.

C. THE PREDICTION-BASED REVERSIBLE WATERMARKING

As described by Lee *et al.* [35] most reversible watermarking techniques require location map for reversibility which increases the additional overhead for a watermarking technique. Thus, to avoid the location map for reversibility and to reduce the additional overhead, the prediction-based reversible watermarking was exploited in the proposed watermarking system.

In this way not only the embedding capacity of the proposed system was increased but also lossless method of conveying the patient information was provided. Recently number of prediction-based reversible watermarking techniques [35]–[37] are reported. In proposed system the prediction-based watermarking as proposed in [35] was utilized and is described as follows:

1) DATA HIDING

1. The input medical image is separated into ROI and RONI regions by applying Algorithm 1.

Algorithm 1 Segmentation Algorithm

Input: CT Scan image
Output: Segmented image

Procedure *segmentation*
Read host image
Find the mean of the all pixels values of input image and consider this mean value as threshold ***T1***
Based on ***T1*** divide the all pixels into two groups. If pixel value is greater than, ***T1*** consider it object pixel and background pixel otherwise.
Calculate the sum of all pixels and number of pixels in each category, and find the average of objects (***AVGO***) and average of backgrounds (***AVGB***)
Find new threshold ***T2***, by calculate the average of ***AVGO*** and ***AVGB***
Repeat these steps until new threshold (***T2***) becomes equal to old threshold ***(T1)***
Finally apply the last found threshold ***T2*** and make all pixels white if pixel value is greater than ***T2***
Set the seed values.
Perform the connectivity and topological analysis using the seed values and produce the tagged image.
Now turn those pixels and neighbours white which are not tagged.
Finally display the segmented image.
End procedure

2. Each pixel of RONI is scanned in raster fashion by excluding the first row and first column and pixel X, is

predicted by using Eq 1:

$$X'(i,\ j) = \left\lfloor \frac{X(i-1,\ j) + X(i,\ j-1)}{2} \right\rfloor, \quad (1)$$

where $\lfloor . \rfloor$ denotes floor function. The prediction error d is found by Eq. 2:

$$d = \left| X(i,\ j) - X'(i,\ j) \right|, \quad (2)$$

3. For each RONI pixel, according to predefined threshold T, d is classified into two categories: $d \leq T$ and $d > T$, where category 1 carries two bits of hidden information b and category 2 does not. *Category 1:* If $d \leq T$ then watermarked pixel value is found by Eq. 3:

$$X^w(i,\ j) = \begin{cases} X'(i,\ j) + 4\,d + b, & \text{if } X'(i,\ j) \leq X(i,\ j) \\ X'(i,\ j) - 4\,d - b, & \text{otherwise.} \end{cases}, \quad (3)$$

where $b \in \{0,\ 1,\ 2,\ 3\}$ denotes two bits of watermark information.
Category 2: If $d > T$ then prediction error is simply shifted by $\Delta_{\text{withnodata embedded}}$ in it and watermarked pixel is obtained by Eq. 4:

$$X^w(i,\ j) = \begin{cases} X'(i,\ j) + \Delta, & \text{if } X'(i,\ j) \leq X(i,\ j) \\ X'(i,\ j) - \Delta, & \text{otherwise.} \end{cases}, \quad (4)$$

where $\Delta = 3T + 3$

4. The parameter T, will be communicated to the decoder.

2) EXTRACTION AND RECOVERY PROCEDURE

To extract the watermark information and restoring the watermarked image to its pristine state following procedure will be adopted and is explained below:

1. The received image is segmented into ROI and RONI.
2. Each pixel of RONI is scanned in raster fashion by excluding the first row and first column and pixel X, is predicted by using Eq. 5:

$$X'(i,\ j) = \left\lfloor \frac{X^w(i-1,\ j) + X^w(i,\ j-1)}{2} \right\rfloor, \quad (5)$$

3. The prediction error d^w is calculated using Eq. 6:

$$d^w = \left| X^w(i,\ j) - X'(i,\ j) \right|, \quad (6)$$

4. For each watermarked RONI pixel according a predefined threshold T, d^w is classified into two categories $d^w \leq 4T + 3$ and $d^w > 4T + 3$

Category 1: If $d^w \leq 4T + 3$ then hidden information (two watermark bits) are extracted by Eq. 7:

$$b = d^w - 4 \left\lfloor \frac{d^w}{4} \right\rfloor, \quad (7)$$

and the original pixel $X(i, j)$ is restored by Eq. 8:

$$X(i,\ j) = \begin{cases} X'(i,\ j) + \left\lfloor \frac{d^w}{4} \right\rfloor, & \text{if } X'(i,\ j) \leq X^w(i,\ j) \\ X'(i,\ j) - \left\lfloor \frac{d^w}{4} \right\rfloor, & \text{otherwise.} \end{cases}, \quad (8)$$

FIGURE 3. The fragile watermark.

Category 2: If $d^w > 4T + 3$, then there will be no any watermark extraction and the original pixel is restored by Eq. 9:

$$X(i,\ j) = \begin{cases} X'(i,\ j) - \Delta, & \text{if } X'(i,\ j) \leq X^w(i,\ j) \\ X'(i,\ j) + \Delta, & \text{otherwise.} \end{cases}, \quad (9)$$

3) UNDERFLOW AND OVERFLOW PROBLEM

In 8-bit gray-level images, the minimum gray level in the image is 0 and the maximum gray level is 255. These values can go beyond their limits when the watermarked information is implanted in the 8-bit gray-level medical image. For example, 0 can become a –ve value and 255 gray level can become more than 255. The extension of 0 gray value towards negative value is called underflow and extension of gray level 255 to some value greater than 255 is called overflow. The shrinkage of both ends is exploited by narrowing down Δ value in our proposed system. Thus, the histogram of the original image which is in the range of [0 255] becomes $[\Delta 255 - \Delta]$ after adjusting the pixel values.

IV. PROPOSED METHOD

A simple medical image watermarking system is presented, which is based on image segmentation, LSB method and prediction-based reversible watermarking. The system divides the host image in the ROI and RONI region automatically by using the segmentation algorithm. It implants a fragile watermark in the ROI to check the integrity of received image, while it embeds a composite robust watermark in the RONI which ensures the confidentiality of patient data as well as copyright protection of medical image. The system introduces less distortion in the host image by keeping the visual quality of the watermarked image at a high level. The system uses the prediction-based reversible watermarking for embedding the recovery information of ROI into RONI, thus it does not require any location map or other additional external information for reversibility. The explanation of implanted watermarks in the proposed system is given as under:

Fragile Watermark (*FW*): The *FW* is a binary pattern as shown in Fig. 3. The *FW* is created by using the Microsoft Paint Tool.

Algorithm 2 Embedding

1 Apply segmentation procedure to get the ROI and RONI.
2 Separate the LSBs of ROI and store in separate store.
3 Generate fragile watermark and robust watermark.
4 Replace the LSBs of ROI with fragile watermark to get watermarked ROI.
5 For each pixel of RONI, repeat process untill all watermark information is embedded in RONI.
6 Calculate prediction $X'(m, n)$ using Eq. (1).
7 Calculate prediction error d using Eq. (2).
8 **If** $d \leq T$
9 If $X'(m, n) \leq X(m, n)$ then $X^w(m, n) = X'(m, n) + 4d + b$
10 Else $X^w(m, n) = X'(m, n) - 4d - b$
11 **Else If** $d > T$
12 If $X'(m, n) \leq X(m, n)$ then $X^w(m, n) = X'(m, n) + \Delta$
13 Else $X^w(m, n) = X'(m, n) - \Delta$
14 **End If**

Algorithm 3 Extraction and Recovery Algorithm

1 Apply segmentation procedure on the watermarekd image to seperate it into ROI and RONI.
2 Extract the LSBs of watermarked ROI for obtaining FW.
3 Calculate prediction $X'(m, n)$ using Eq. (5).
4 Calculate prediction error d^w using Eq. (6).
5 Now keeping in view the length of the watermark, extract the watermark information from RONI pixels using Eq(7):
6 $b = d^w - 4\,(floor(d^w/4))$
7 Based on the value of dw restore each pixel of RONI by using Eq(8) and Eq(9):
8 **If** $d^w \leq 4T + 3$
9 If $X'(m, n) \leq X^w(m, n)$ then $X(m, n) = X'(m, n) + (d^w/4)$
10 Else $X^w(m, n) = X'(m, n) - (d^w/4)$
11 **Else If** $d > 4\ T+3$
12 If $X'(m, n) \leq X^w(m, n)$ then $X(m, n) = X'(m, n) - \Delta$
13 Else $X(m, n) = X'(m, n) + \Delta$
14 **End If**

Robust Watermark (*RW*): The *RW* is composed of four different watermarks as shown in Fig. 4: (i) The Patient record (*PR*) presents the particulars about the patient such as Name, Age, Sex, etc. *PR* is converted in the binary vector before embedding by following the procedure as explained in [38], [39]. A total of 1024 bits are used for *PR*. (ii) The doctor's ID (*DI*) is the unique string of 16 characters to identify the creator of the medical image. The length of *DI* becomes 128 bits after converting the character information of *DI* in a binary. (iii) Hospital logo (*HL*) is the binary logo which is used for copyright protection of medical image. The main purpose of *HL* is to identify the hospital which owns the medical image. The *HL* is shown in Fig. 5. The size of *HL* is 64×64 which produces the binary vector of 4096 bits. The LSB information (*LI*) is the collection of LSBs related to the first bit plane of ROI. The length of *LI* depends upon the size of ROI in the host image. The larger the size of ROI, the higher will be the length of *LI* and vice versa. *DI*, *HL*, *DI,* and *LI* are concatenated to form a binary vector. Later this vector is EX-ORed with some pseudo-random generated binary vector of the same size based on the key to increase the security of robust watermark. This key will be communicated to the decoder for extracting the watermark information.

The proposed system is comprised of two main phases: The embedding phase and the extraction and recovery phase. Each phase is further described under:

A. THE EMBEDDING PHASE

In this phase, the cover image is first divided in ROI and RONI regions by following the Algorithm 1. After division, the watermark casting process is done separately in these two regions. The complete embedding process is shown in the block diagram as given in Fig. 6. Each step of algorithm used for watermark casting process is further described as given in Algorithm 2.

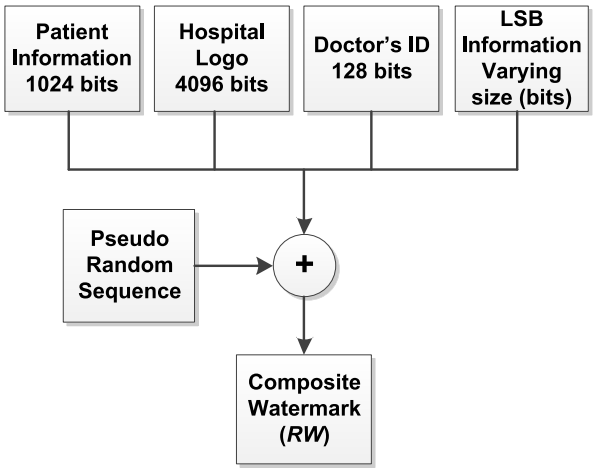

FIGURE 4. The composite robust watermark.

FIGURE 5. The hospital logo.

B. THE EXTRACTION AND RECOVERY PHASE

The block diagram of extraction and recovery process is shown in Fig. 7. Few steps of extraction and recovery process are same as the embedding process. The extraction and recovery process is given in Algorithm 3.

V. EXPERIMENTAL RESULTS AND DISCUSSIONS

The experimental results of both the embedding and the extraction phases are described in the following sections.

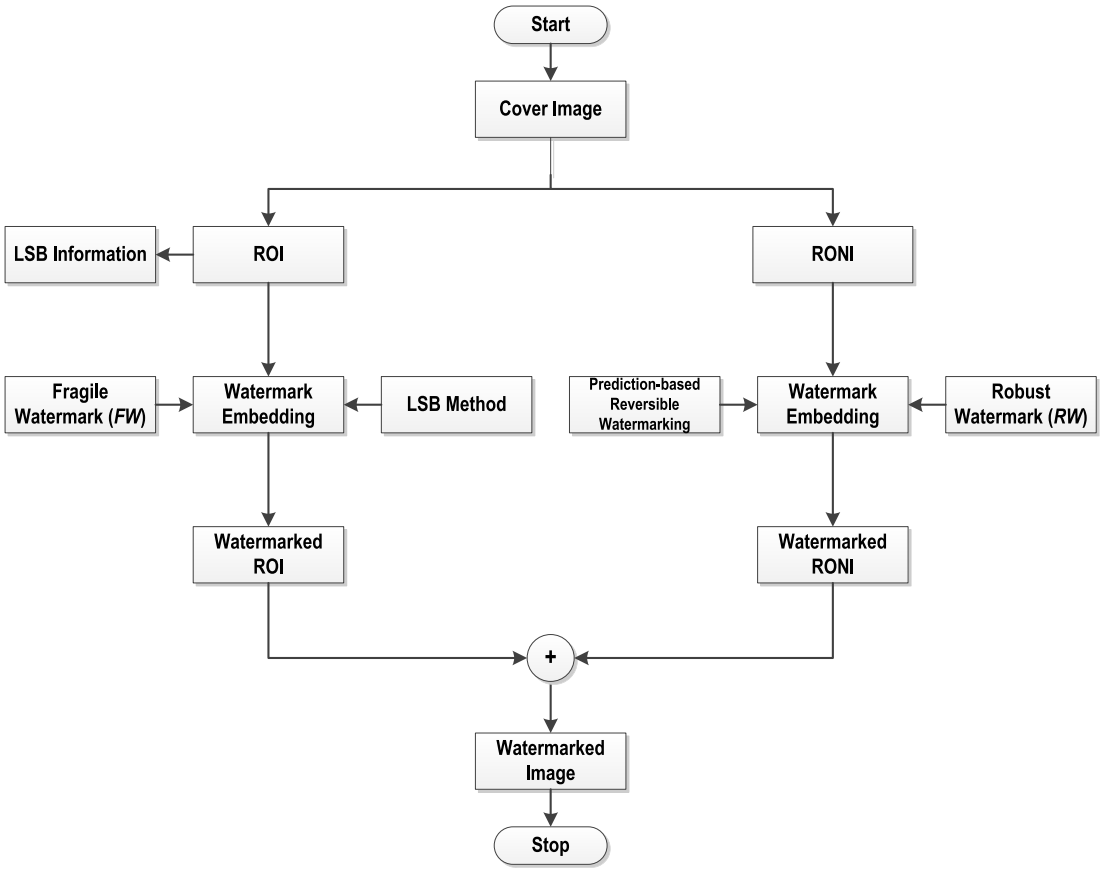

FIGURE 6. Block diagram of embedding algorithm.

A. THE RESULTS OF EMBEDDING PHASE

The results of embedding phase are described below.

1) EXPERIMENAL SETUP

The CT scan medical images are used as a special case for our experimental work. However, the proposed system can be applied to any imaging modality such as MRI, XRAY, Ultrasound, etc. In that case, selection of ROI will be the choice of the doctor and how he/she selects the ROI, either manually or automatically. The simulations are carried out on the dataset as portrayed in Table 1. Few experimental results using the dataset of the patient having ID L07201201 in Table 1 are shown in Fig. 8. This dataset consists of 60 slices having a slice thickness of 4.0 mm. The medical images were received from the radiology departments of two different hospitals. About 701 images of 10 cases were received from the Radiological Department of Akron University, Ohio, USA and 850 images of 12 cases were received from AGA Khan Medical University, Karachi, Pakistan. All images were 8-bit gray level images and were resized to 256 × 256 pixels for simulations.

2) SEGMENTATION OF INPUT IMAGE AND EMBEDDING THE WATERMARKS

Algorithm 1 was applied to input CT scan image to divide it into ROI and RONI. Fig. 9 shows the ROI and RONI of the early, middle and end area of lung parenchyma. For showing the early, middle and end parts of lung parenchyma different slices are selected from the slices shown in Fig. 8. For example, Slice#9 is selected for showing early lung area, slice#25 is selected for showing middle lung area and slice#49 is selected for showing the end of the lung area. Then, *FW* and *RW* were generated and embedded in ROI and RONI areas respectively. During segmentation, a binary mask was created for helping the embedder to differentiate between ROI and RONI regions while casting the watermark in the host image. In mask, all pixels belonging to the ROI region are set as white, while all pixels belonging to RONI are set as black. The mask is shown in Fig. 10. *FW* is implanted in

TABLE 1. Datasets of CT scan images used for experiments.

S.No.	Patient-ID	Number of Slices	Slice Thickness (mm)
1	L06201201	56	3.0
2	L07201201	60	4.0
3	L08201201	68	1.0
4	L01201401	70	2.0
5	L02201501	65	4.0
6	L03201501	99	5.0
7	L06201501	101	0.4
8	L05201501	67	0.3
9	L04201501	75	0.2
10	L03201501	40	0.1

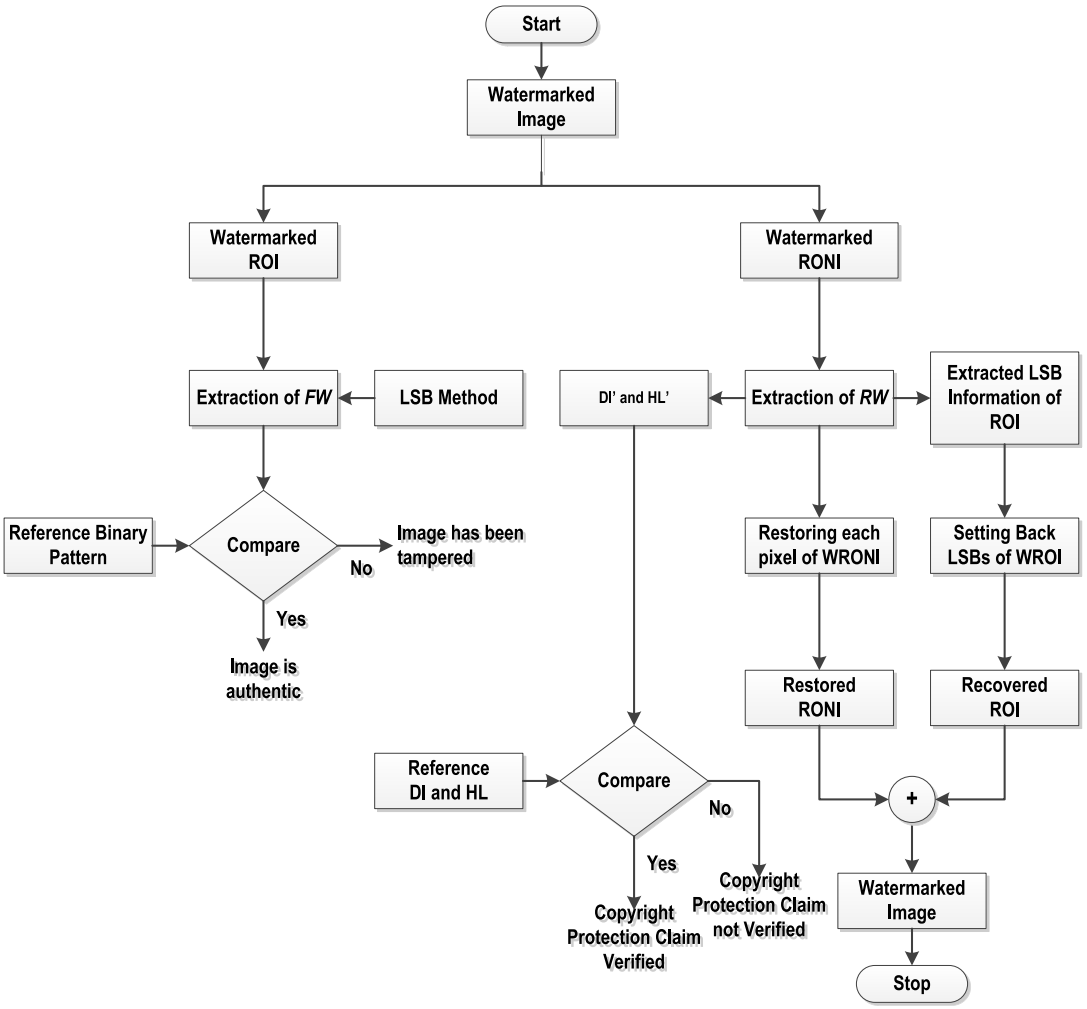

FIGURE 7. Block diagram of extraction algorithm.

the ROI by replacing its LSBs by keeping in view the white area of the binary mask, while *RW* is implanted in the RONI by considering the black area of mask. The prediction-based reversible watermarking is employed for inserting the *RW* in the RONI. The threshold value of T = 1 is assumed for embedding. The T is capacity parameter. Keeping smallest threshold will provide enough expandable pixels to embed the payload. The results after embedding the watermarks in both ROI and RONI are shown in Fig. 11. In Fig. 11, column (a) depicts the host image, column (b) shows the watermarked image with PSNR value measured after embedding the watermarked information, and column (c) shows the difference between the host image and watermarked image. Table 2 depicts the embedding results of the model patient's case containing 60 slices. In Table 2, columns 1-7 represent the slice #, segmentation time, number of bits containing *FW*, number of bits containing *RW*, the total number of bits implanted in host image, payload and PSNR respectively. The PSNR values are calculated using the Eq. 10 and Eq. 11.

$$PSNR = 10\log_{10}\frac{R^2}{MSE}, \tag{10}$$

$$MSE = \frac{\sum_{M,N}[I(m,n) - I^w(m,n)]^2}{M \times N}, \tag{11}$$

3) SEGMENTATION TIME

The segmentation time for each slice is shown in column 2 of Table 2. The segmentation time varies between 10.8866 seconds and 13.1610 seconds. On average, the segmentation time is 11.35 seconds. The line graph given in Fig. 12 depicts the segmentation time for each slice. The segmentation for each slice is more or less the same. This is because the segmentation process does not dependent on the size of ROI. The segmentation algorithm checks the whole image pixel by pixel even if there is no ROI in the input image.

4) SIZE OF FW AND RW

The columns 3-4 of Table 2, show the number of pixels containing *FW* and *RW* watermarks. The size of these watermarks is actually depends on the size of ROI in the input image. The size of ROI varies from top to bottom in the lung CT scan images. This is due to the structure of lung parenchyma in the human body. It can be observed

TABLE 2. Simulation results after embedding phase.

Slice # (1)	Segmentation time (Seconds) (2)	*FW* (bits) (3)	*RW* (bits) (4)	Total no of bits embedded (5)	Payload (bpp) (6)	PSNR (dB) (7)
1	11.5564	0	6144	6144	0.093781	56.3612
2	11.3158	0	6144	6144	0.093781	56.3604
3	11.9053	0	6144	6144	0.093781	56.2361
4	11.7697	0	6144	6144	0.093781	56.1706
5	11.1209	0	6144	6144	0.093781	56.1829
6	11.0436	1659	7803	9462	0.144409	54.5956
7	11.0672	3287	9431	12718	0.194092	53.4360
8	11.1377	4661	10805	15466	0.236023	52.5912
9	11.0732	6202	12346	18548	0.283051	51.8364
10	11.1824	7598	13742	21340	0.325653	51.1132
11	11.1421	8931	15075	24006	0.366333	50.5786
12	10.9377	10262	16406	26668	0.406952	50.0069
13	11.1272	11536	17680	29216	0.445831	49.6439
14	11.1559	12458	18602	31060	0.473969	49.3940
15	10.9419	13022	19166	32188	0.491180	49.2786
16	10.9464	13488	19632	33120	0.505402	49.0648
17	11.1987	14002	20146	34148	0.521088	48.9104
18	11.1513	14486	20630	35116	0.535858	48.8199
19	11.4493	14791	20935	35726	0.545166	48.7170
20	11.0984	15040	21184	36224	0.552765	48.6418
21	10.8827	15222	21366	36588	0.558319	48.5836
22	10.8866	15030	21174	36204	0.552460	48.6422
23	11.1605	15429	21583	37022	0.564941	48.5822
24	11.1053	15366	21510	36776	0.562714	48.5965
25	11.1504	15135	21279	36414	0.555664	48.6530
26	11.3058	14977	21121	36098	0.550842	48.6548
27	11.5936	14800	20944	35744	0.545441	48.6637
28	11.8838	14671	20815	35486	0.541504	48.7283
29	11.2522	14461	20605	35066	0.535095	48.8223
30	11.1706	14203	20347	34550	0.527222	48.8938
31	11.2868	13975	20119	34094	0.520264	48.9657
32	11.7189	13608	19752	33360	0.509064	48.9883
33	11.4269	13187	19331	32518	0.496216	49.0693
34	11.5679	13095	19239	32334	0.493408	49.1353
35	11.5404	12830	18974	31804	0.485321	49.2693
36	11.6905	12714	18858	31572	0.481781	49.3071
37	11.8728	12678	188222	31500	0.480682	49.3089
38	12.2462	12884	19028	31912	0.486969	49.3425
39	12.2120	12881	19025	31906	0.486877	49.3823
40	11.8808	12103	18247	30350	0.463135	49.4824
41	11.6334	11580	17724	29304	0.447174	49.5436
42	11.6303	10567	16711	27278	0.416260	49.8800
43	11.5337	9708	15852	25560	0.390045	50.2496
44	11.4200	9131	15275	24406	0.372437	50.4544
45	11.3360	7857	14001	21858	0.333557	50.9438
46	11.2350	6628	12772	19400	0.296051	51.5101
47	11.1850	5363	11507	16870	0.257446	52.1551
48	11.3653	4044	10188	14232	0.217194	52.8081
49	11.1218	2689	8833	11522	0.175842	53.5918
50	11.0638	1737	7881	9618	0.146790	54.3990
51	11.0083	1220	7364	8584	0.131012	54.8176
52	10.9046	463	6607	7070	0.107910	55.5742
53	10.9728	0	6144	6144	0.093781	56.0286
54	11.0709	0	6144	6144	0.093781	56.2019
55	11.2644	0	6144	6144	0.093781	56.1090
56	11.1756	0	6144	6144	0.093781	56.0225
57	11.1142	0	6144	6144	0.093781	55.9730
58	11.4827	0	6144	6144	0.093781	56.0532
59	11.2062	0	6144	6144	0.093781	56.0730
60	13.1610	0	6144	6144	0.093781	56.1951

from Table 2, column 3, that the number of pixels in the start and end slices is smaller than the slices belong to the middle part of the lung. The bar graph shown in Fig. 13 also reveals such fact of the lung CT scan images of the human body. Due to this fact, less number of watermark bits are implanted in starting and end slices whereas the

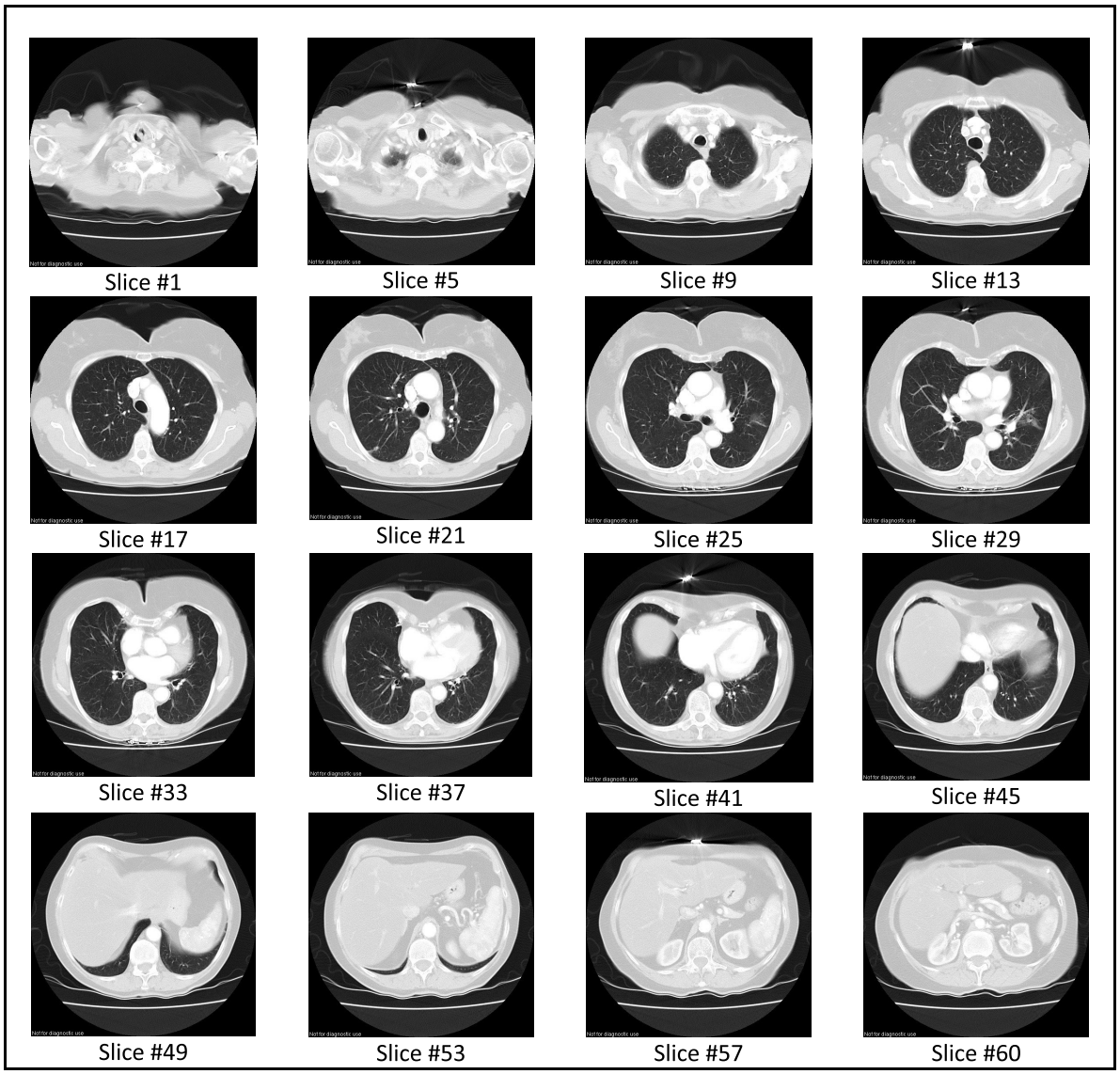

FIGURE 8. CT scan images used in simulations.

large number of watermark bits are implanted in middle slices.

5) IMPERCEPTIBILITY

The columns 6-7 in Table 2, represent the payload (which is the amount of watermarked information embedded per pixel in the input image) and PSNR (which is the measure of imperceptibility). Imperceptibility means that how much input image is degraded after embedding the payload. The benchmark value of 40 dB is considered acceptable for the human visual system (HVS). There is always a tradeoff between the payload and imperceptibility. The higher the value of payload, the lower will be the value of PSNR and vice versa. This observation can also be checked from Fig. 14. The graph shown in Fig. 14 reveals that the slices possess smaller ROI, it allows fewer bits to be embedded and thus report higher values of PSNR. In contrast, the slices possess a larger ROI area, it allow a high amount of bits to be embedded and reports smaller values of PSNR.

B. THE RESULTS OF EXTRACTION AND RECOVERY PHASE

To check the integrity of recovered image, first, the segmentation procedure was applied on the received image to get the watermarked ROI and RONI regions. Then watermarks were extracted from both regions. To extract the *FW*, LSB of each pixel of ROI was collected. While for extracting *RW* prediction-based reversible watermarking was employed on RONI. During this extraction process each pixel of RONI was also recovered. The *RW* extracted from RONI was EX-ORed with the same pseudo-random sequence that was generated at the time of embedding to get back the original *RW*. Furthermore, *RW* was divided into four different watermarks (*PR'*, *DI'*, *HL'* and *LI'*) as per their pre-defined lengths. The binary pattern was created from extracted binary vector *LI'*

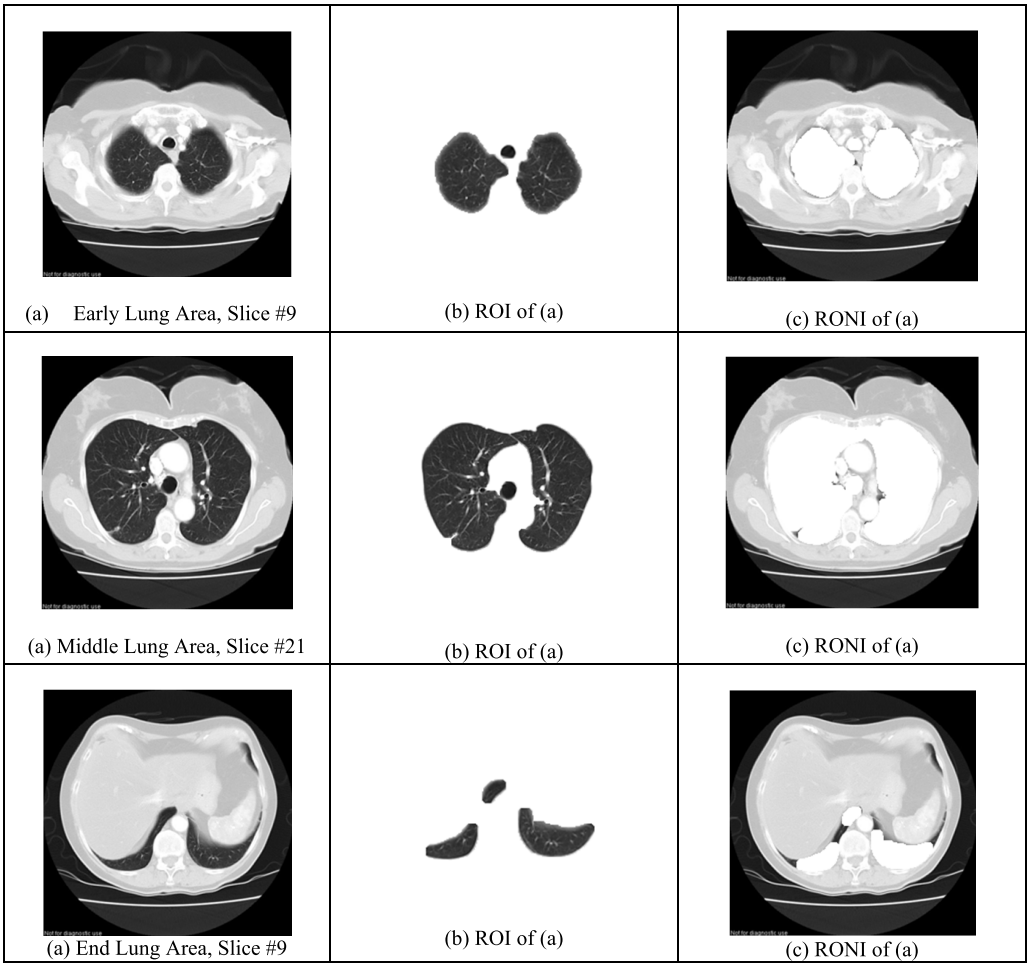

FIGURE 9. ROI and RONI of early, middle and end part of lung parenchyma.

and was compared with reference binary pattern *LI*. With visual inspection, it was found that the extracted binary pattern was exactly the same as reference binary pattern. The extracted binary pattern is shown in Fig. 15. There may be the possibility of error in visual inspection of the binary patterns. Therefore, extracted LSB information (*LI'*) was compared with reference LSB information (*LI*) using the Normalized Hamming Distance (NHD) matric [33]. The NHD defines that, the lower the value of the distance between embedded and extracted watermark, then the higher will be the accuracy of watermark. The distance of zero was found between the original *LI* and extracted *LI'*. Thus it was concluded that the received image has not undergone any type of tampering during transmission.

Similarly extracted *DI'* and *HL'* were also compared with their reference counterparts *DI* and *HL* for verifying the copyright claim of the received image. The extracted *PI'* was passed under the reverse process to get back the patient information in alphabetic characters. For restoring the original ROI, every LSB of watermarked ROI was set back with the extracted LSB information (*LI'*).

Finally, both restored regions were combined to bring back the input image to its pristine state.

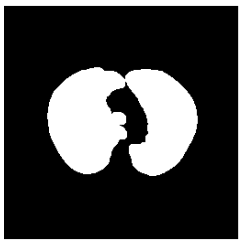

FIGURE 10. The binary mask.

C. COMPARISON WITH RELEVANT TECHNIQUES

The comparison of our proposed system with other reversible medical image watermarking schemes is given in Table 3. The table portrays that the proposed system performs better than the schemes [22], [23] in terms of segmentation because these schemes segment the input image into ROI and RONI manually. Thus there is a potential threat of loss of watermarked information if the selection of ROI and RONI is not exacly the same at the time of embedding and extraction process. In contrast, the proposed system uses the automatic method of segmentation which takes about 10 to 11 seconds for segmenting the host image into ROI and RONI. The segmentation algorithm takes care while embedding the watermark information in RONI by leaving five pixel boundary around the ROI.

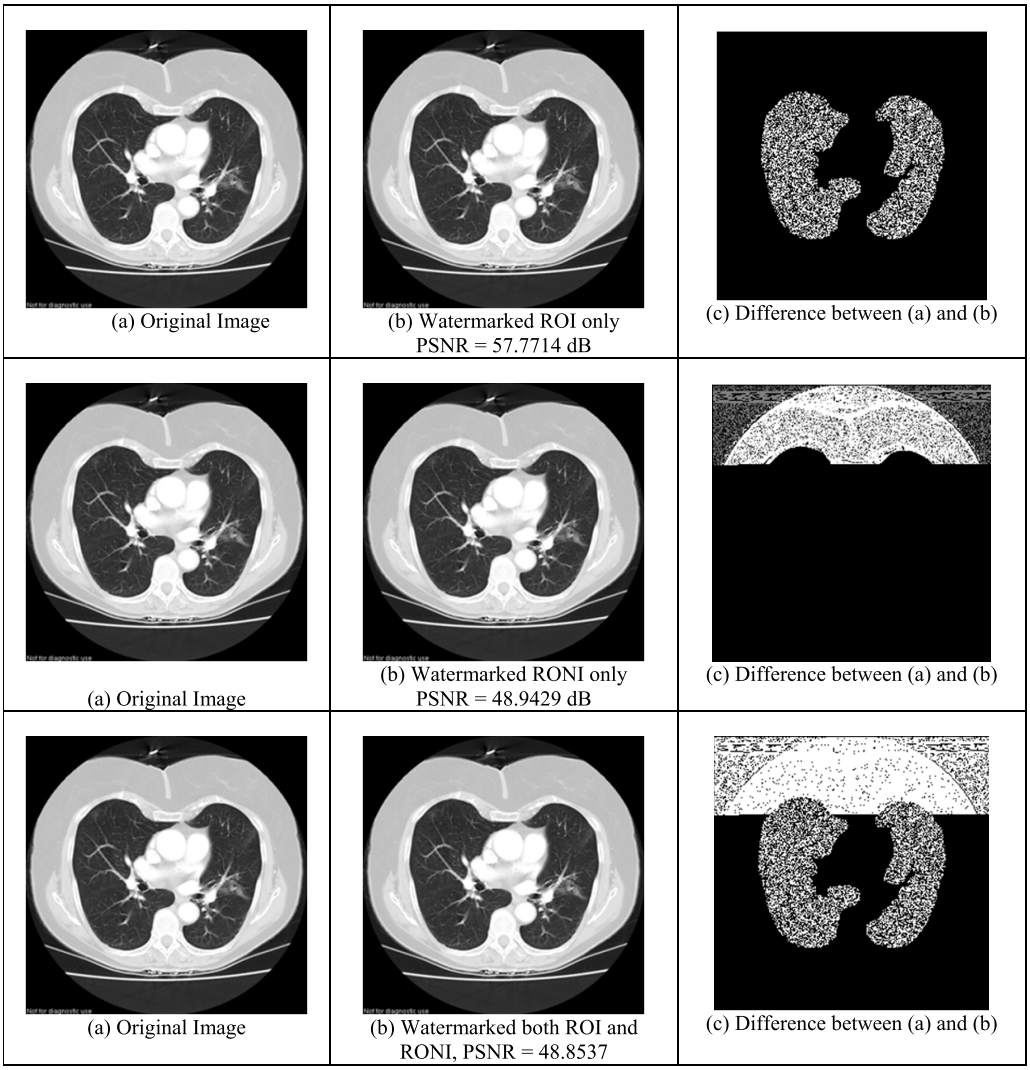

FIGURE 11. **(a) Original images (b) Watermarked images (c) Residual images (difference between original and watermarked image).**

Thus there will not be the loss of any information due to segmentation when the host image is segmented in a spatial domain.

In terms of location map requirement or additional overhead of coordinates information required for selecting ROI at the receiving end, the proposed system is better than techniques [26], [28] because these techniques require location map for recovery as well as for extracting the watermark information. The proposed system uses prediction-based reversible watermarking that does not require a location map for reversibility.

In terms of reversibility, the proposed system outperforms in comparison to schemes described in [23], [26]. Because these schemes only restore the ROI region and not recover the whole image. Thus these techniques are not fully reversible. The proposed system recovers both ROI and RONI regions. Thus proposed system is capable of restoring the whole image to its pristine state.

In terms of capacity, the proposed system is better than the schemes [22], [24], [26]–[28], becausee these schemes do not provide a high quality of watermarked images despite of low embedding payload. The proposed system reports the high values of PSNR despite high payload values as compared to [22], [24], [26]–[28].

In terms of the visual quality of watermarked image, the proposed system is better than [22], [23], [25]–[28], [29], [30]. It is because these schemes do not give high values of PSNR as compared to the proposed system.

In addition, regarding the restriction of the size of ROI as given in [23], the technique cannot be applied tothe images where ROI size is greater than 20% of the whole image. If we check the simulation results in column 3 of Table 2, the maximum number of pixels in ROI in the model database, slice#23 is 15429 pixels which is 23.5% of the whole host image. Thus there is 76.5% of the whole image is available for embedding ROI information.

TABLE 3. Comparison of proposed method with different relevant techniques.

Scheme	Year	Segmentation Process	Embedding Region	Embedding Technique	Location Map ?	Reversible ?	Payload (bpp)	PSNR (dB)
Thabit et. al. [22]	2015	Manual	ROI RONI	SLT	No	Yes	0.1932 – 0.2203	32.5856 – 42.4724
Eswaraiah etl. al. [23]	2015	Manual	RONI only	IWT	No	Yes only ROI	Not defined	51.73
Selvam et. al. [24]	2017	No	Whole image	IWT DGT	No	Yes	0.0625 – 0.2500	60.42 - 65.23
Parah et. al. [25]	2017	No	Whole image	PTB Conversion ISBB	No	Yes	0.40 – 0.75	46.36 – 49.10
Gao et. al. [26]	2017	Automatic	ROI RONI	HS LSB	Yes	Only ROI	0.0760 – 0.3530	24.50 - 0.45
Balasamy et. al. [27]	2018	No	Whole image	DWT PSO	No	Yes	0.1467	49.01
Yang. et. al. [28]	2018	Automatic	ROI RONI	HS	Yes	Yes	0.01 – 3.0	14.74 – 23.06
Atta-ur-Rehman et. al. [6]	2018	No	Whole Image	Residue with chaotically selected pixels	No	Yes	Not presented	72.28
Xiyao Liu et. al [29]	2019	Automatic	Whole image	RDM SLT SVD	No	Yes	Not presented	41.2995
Swaraja et. al. [30]	2020	Automatic	ROI RONI	DWT PSBFO	No	Yes	Not presented	33.18
Proposed	---	Automatic	ROI RONI	Prediction error expanding	No	Yes	0.0937 – 0.5556	48.6530 – 56.3612

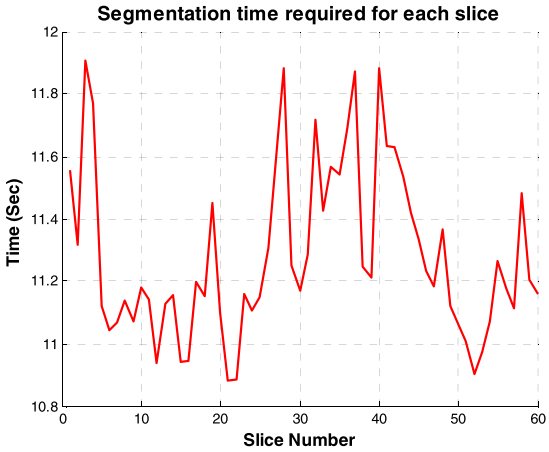

FIGURE 12. Segmentation time required for each slice of image database of model patient.

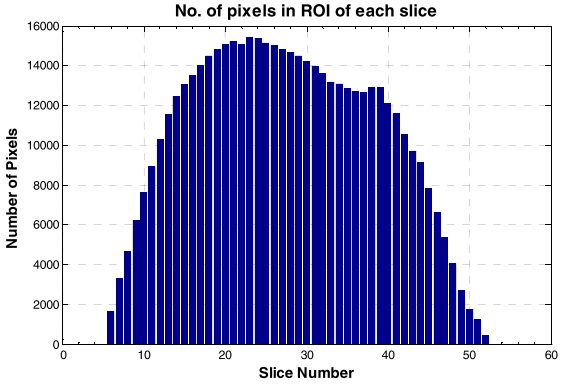

FIGURE 13. Behaviour of ROI in each slice of model patient.

Thus proposed system has not any ROI size restriction. Also, the technique reported by Abokhdair and Manaf [37] sends the vertices information of polygon marked as ROI

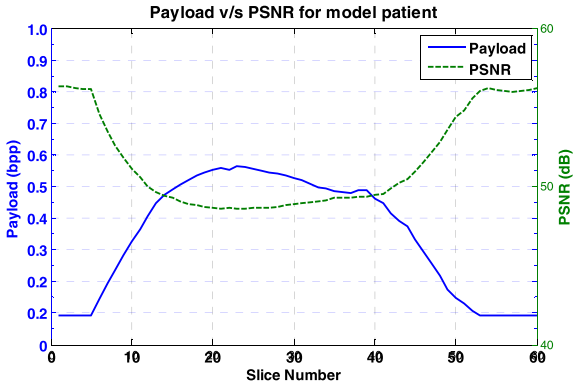

FIGURE 14. Payload v/s PSNR graph.

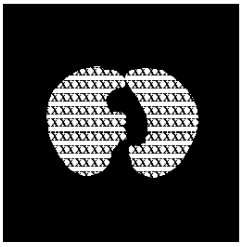

FIGURE 15. The extracted *FW* (binary pattern).

at the time of embedding to the decoder for extracting the watermark information. In contrast, the proposed system segments the host image into ROI and RONI regions by using the segmentation algorithm, which divides the host image 100% accurately in ROI and RONI regions at the time of embedding and extraction the watermark information. Thus, there is no need of sending any additional information as overhead to the decoder for extracting the watermark information. Thus, the proposed system outperforms than the technique described in [37].

VI. CONCLUSION

In this paper, we have presented a reversible medical image watermarking system for content authentication and copyright protection of CT scan medical images produced in the teleradiology environment. The proposed system automatically segments the host image into ROI and RONI regions by using the segmentation algorithm. Thus, the proposed system does not need any additional information of vertices used in other techniques for defining the ROI at the receiving end. LSB substitution method is used to implant the watermark in ROI while prediction-based reversible watermarking is used to implant the watermark in the RONI region. The exact host image can be brought to its pristine state after extracting the watermark information. The need for location map is not required for reversibility. Thus, the proposed system increases the embedding capacity. The proposed system embeds the hidden information in both ROI and RONI regions by keeping the visual quality of the watermarked image at very high level by yielding the PSNR values in the range $\{48 - 56\}$ dB. This introduces the distortion less noticeable to human visual perception. The proposed system facilitates the radiologist to transmit the CT scan images to other radiologists without the fear of loss of medical information.

The content integrity is ensured by using Fragile watermarking while the confidentiality of patient information is ensured by using Robust watermarking. The computational cost of the proposed system is also very low. Thus, the proposed system leads to a very efficient system which provides complete authentication and copyright protection of CT Scan medical image databases at a very low cost. The proposed system can be used by low budget hospitals. However, the robust watermark implanted in RONI is not so robust and can be vulnerable to any legitimate or illegitimate attacks. The future direction of our research is to develop a medical image watermarking system that can sustain the legitimate attacks while illegitimate attacks can be recognized if the watermarked image goes under any unlawful assault.

REFERENCES

[1] A. Ustubioglu and G. Ulutas, "A new medical image watermarking technique with finer tamper localization," *J. Digit. Imag.*, vol. 30, no. 6, pp. 665–680, Dec. 2017.

[2] H. Nyeem, W. Botes, and C. Boyd, "A review of medical image watermarking requirements for technology," *J. Digit. Imag.*, vol. 26, no. 2, pp. 326–343, 2013.

[3] P. Ruotsalainen, "Privacy and security in teleradiology," *Eur. J. Radiol.*, vol. 73, no. 1, pp. 31–35, Jan. 2010.

[4] F. Prior, M. L. Ingeholm, B. A. Levine, and L. Tarbox, "Potential impact of HITECH security regulations on medical imaging," in *Proc. Annu. Int. Conf. IEEE Eng. Med. Biol. Soc.*, Piscataway, NJ, USA, Sep. 2009, pp. 2157–2160.

[5] S. A. Asabe, N. D. Oye, and G. Mondag, "Hospital patient database management system: A case study of general hospital north-bank Makurdi–Nigeria," *Compusoft*, vol. 2, no. 3, pp. 65–72, 2013.

[6] Atta-ur-Rehman, K. Sultan, N. Aldhafferi, A. Alqahtani, and M. Mahmud, "Reversible and fragile watermarking for medical images," *Comput. Math. Methods Med.*, vol. 2018, pp. 1–7, Jul. 2018.

[7] A. F. Qasim, R. Aspin, F. Meziane, and P. Hogg, "ROI-based reversible watermarking scheme for ensuring the integrity and authenticity of DICOM MR images," *Multimedia Tools Appl.*, vol. 78, no. 12, pp. 16433–16463, Jun. 2019.

[8] S. M. Mousavi, A. Naghsh, and S. A. R. Abu-Bakar, "Watermarking techniques used in medical images: A survey," *J. Digit. Imag.*, vol. 27, no. 6, pp. 714–729, Dec. 2014.

[9] N. A. Memon, A. Chaudhry, M. Ahmad, and Z. A. Keerio, "Hybrid watermarking of medical images for ROI authentication and recovery," *Int. J. Comput. Math.*, vol. 88, no. 10, pp. 2057–2071, Jul. 2011.

[10] F. Abbasi and N. A. Memon, "Reversible watermarking for the security of medical image databases," in *Proc. 21st Saudi Comput. Soc. Nat. Comput. Conf. (NCC)*, Riyadh, Saudi Arabia, Apr. 2018, pp. 1–6.

[11] J. M. Zain and A. R. M. Fauzi, "Medical image watermarking with tamper detection and recovery," in *Proc. Int. Conf. IEEE Eng. Med. Biol. Soc.*, Aug. 2006, pp. 3270–3273.

[12] S.-C. Liew and J. M. Zain, "Reversible medical image watermarking for tamper detection and recovery," in *Proc. 3rd Int. Conf. Comput. Sci. Inf. Technol.*, Jul. 2010, pp. 417–420.

[13] S.-C. Liew, S.-W. Liew, and J. M. Zain, "Reversible medical image watermarking for tamper detection and recovery with Run Length Encoding compression," World Acad. Sci., Eng. Technol., Paris, France, 2011, pp. 799–803, no. 50.

[14] J. H. K. Wu, R.-F. Chang, C.-J. Chen, C.-L. Wang, T.-H. Kuo, W. K. Moon, and D.-R. Chen, "Tamper detection and recovery for medical images using near-lossless information hiding technique," *J. Digit. Imag.*, vol. 21, no. 1, pp. 59–76, Mar. 2008.

[15] K.-H. Chiang, K.-C. Chang-Chien, R.-F. Chang, and H.-Y. Yen, "Tamper detection and restoring system for medical images using wavelet-based reversible data embedding," *J. Digit. Imag.*, vol. 21, no. 1, pp. 77–90, Mar. 2008.

[16] O. M. Al-Qershi and B. E. Khoo, "Authentication and data hiding using a reversible ROI-based watermarking scheme for DICOM images," in *Proc. Int. Conf. Med. Syst. Eng. (ICMSE)*, 2009, pp. 829–834.

[17] X. Deng, Z. Chen, F. Zeng, Y. Zhang, and Y. Mao, "Authentication and recovery of medical diagnostic image using dual reversible digital watermarking," *J. Nanosci. Nanotechnol.*, vol. 13, no. 3, pp. 2099–2107, Mar. 2013.

[18] X. Luo, Q. Cheng, and J. Tan, "A lossless data embedding scheme for medical images in application of e-diagnosis," in *Proc. 25th Annu. Int. Conf. IEEE Eng. Med. Biol. Soc.*, Sep. 2003, pp. 852–855.

[19] O. M. Al-Qershi and B. E. Khoo, "Authentication and data hiding using a hybrid ROI-based watermarking scheme for DICOM images," *J. Digit. Imag.*, vol. 24, no. 1, pp. 114–125, Feb. 2011.

[20] O. M. Al-Qershi and B. E. Khoo, "ROI-based tamper detection and recovery for medical images using reversible watermarking technique," in *Proc. IEEE Int. Conf. Inf. Theory Inf. Secur.*, Beijing, China, Dec. 2010, pp. 151–155.

[21] H. Nyeem, W. Boles, and C. Boyd, "Utilizing least significant bit-planes of RONI pixels for medical image watermarking," in *Proc. Int. Conf. Digit. Image Comput., Techn. Appl. (DICTA)*, Nov. 2013.

[22] R. Thabit and B. E. Khoo, "Medical image authentication using SLT and IWT schemes," *Multimedia Tools Appl.*, vol. 76, no. 1, pp. 309–332, Jan. 2017, doi: 10.1007/s11042-015-3055-x.

[23] R. Eswaraiah and E. S. Reddy, "Robust medical image watermarking technique for accurate detection of tampers inside region of interest and recovering original region of interest," *IET Image Process.*, vol. 9, no. 8, pp. 615–625, Aug. 2015.

[24] P. Selvam, S. Balachandran, S. P. Iyer, and R. Jayabal, "Hybrid transform based reversible watermarking technique for medical images in telemedicine applications," *Optik*, vol. 145, pp. 655–671, Sep. 2017.

[25] S. A. Parah, F. Ahad, J. A. Sheikh, and G. M. Bhat, "Hiding clinical information in medical images: A new high capacity and reversible data hiding technique," *J. Biomed. Informat.*, vol. 66, pp. 214–230, Feb. 2017.

[26] G. Gao, X. Wan, S. Yao, Z. Cui, C. Zhou, and X. Sun, "Reversible data hiding with contrast enhancement and tamper localization for medical images," *Inf. Sci.*, vols. 385–386, pp. 250–265, Apr. 2017.

[27] K. Balasamy and S. Ramakrishnan, "An intelligent reversible watermarking system for authenticating medical images using wavelet and PSO," *Cluster Comput.*, vol. 22, no. S2, pp. 4431–4442, Mar. 2019.

[28] Y. Yang, W. Zhang, D. Liang, and N. Yu, "A ROI-based high capacity reversible data hiding scheme with contrast enhancement for medical images," *Multimedia Tools Appl.*, vol. 77, no. 14, pp. 18043–18065, Jul. 2018.

[29] X. Liu, J. Lou, H. Fang, Y. Chen, P. Ouyang, Y. Wang, B. Zou, and L. Wang, "A novel robust reversible watermarking scheme for protecting authenticity and integrity of medical images," *IEEE Access*, vol. 7, pp. 76580–76598, 2019.
[30] K Swaraja, K Meenakshi, and P Kora, "An optimized blind dual medical image watermarking framework for tamper localization and content authentication in secured telemedicine," *Biomed. Signal Process. Control*, vol. 55, Jan. 2020, Art. no. 101665.
[31] B. L. Gujral and S. N. Mali, "ROI based embedded watermarking of medical images for secure communication in telemedicine," *Int. J. Comput. Inf. Eng.*, vol. 6, no. 8, pp. 997–1002, 2012.
[32] N. A. Memon, A. M. Mirza, and S. A. M. Gilani, "Segmentation of lungs from CT Scan images for early diagnosis of Lung Cancer," *Int. J. Med. Health Sci.*, vol. 2, no. 8, pp. 297–302, 2008.
[33] N. A. Memon, Z. A. Keerio, and F. Abbasi, "Dual watermarking of CT scan medical Images for content authentication and copyright protection," in *Proc. Conf. (CCIS)*, vol. 14, F. K. Shaikh and B. S. Chaudhary, Eds. Cham, Switzerland: Springer, 2014 pp. 73–183.
[34] N. A. Memon and S. A. M. Gilani, "NROI watermarking of medical images for content authentication," in *Proc. IEEE Int. Multitopic Conf.*, Karachi, Pakistan, Dec. 2008, pp. 106–110.
[35] C.-F. Lee, H.-L. Chen, and H.-K. Tso, "Embedding capacity raising in reversible data hiding based on prediction of difference expansion," *J. Syst. Softw.*, vol. 83, no. 10, pp. 1864–1872, Oct. 2010.
[36] H. W. Tseng and C. P. Hsieh, "Prediction-based reversible data-hiding," *J. Inf. Sci.*, vol. 179, no. 14, pp. 2460–2469, 2010.
[37] N. O. Abokhdair and A. A. Manaf, "A preiction-based reversible watermarking for MRI images," *Int. J. Comput., Elect., Automat., Control Inf. Eng.*, vol. 7, no. 2, pp. 328–331, 2013.
[38] K. A. Navas, S. A. Thampy, and M. Sasikumar, "EPR hiding in medical images for telemedicine," in *Proc. World Acad. Sci., Eng. Technol.*, Rome, Italy, 2008, pp. 292–295.
[39] N. A. Memon and S. A. M. Gilnai, "Watermarking of chest CT san medical images for content authentication," *Int. J. Comput. Mathetmatics*, vol. 88, no. 2, pp. 265–280, 2010.

NISAR AHMED MEMON received the bachelor's degree in computer systems engineering from Mehran University, Jamshoro, Pakistan, in 1989, the M.S. degree in computer engineering from the Ghulam Ishaq Khan Institute (GIKI), Pakistan, in 2005, and the Ph.D. degree in computer engineering from the GIK Institute, Pakistan, in 2010. He is currently working as an Assistant Professor with the College of Computer Sciences and Information Technology (CCSIT), King Faisal University, Saudi Arabia. His current research interests include digital image processing, digital image watermarking, pattern recognition, data authentication, and cryptography. He has published more than 40 research articles in international journals and conferences in the field of image processing, data authentication, medial image watermarking, data security, and bioinformatics.

ALI ALZAHRANI (Member, IEEE) received the B.Eng. degree in computer engineering from Umm Al-Qura University, Mecca, Saudi Arabia, and the M.Sc. and Ph.D. degrees in computer engineering from the University of Victoria, BC, Canada, in 2015 and 2018, respectively. He is currently an Assistant Professor with the Department of Computer Engineering, King Faisal University. His research interests include hardware security, encryption processors, image processing, and systems-on-chip.